Admittance-Based Aggregated Modeling for Resonance Analysis of Multi-Converter Systems in Nodal-Based EMT Simulators

Arash Safavizadeh
Department of Electrical and Computer Engineering
University of British Columbia
Vancouver, Canada
arash.safavizadeh@ece.ubc.ca

MohammadSadegh KhajueeZadeh
Department of Electrical and Computer Engineering
University of British Columbia
Vancouver, Canada
mohammadkhajuee@ece.ubc.ca

Seyyedmilad Ebrahimi
School of Electrical Engineering and Computer Science
Washington State University
Pullman, United States
s.ebrahimi@wsu.edu

Juri Jatskevich
Department of Electrical and Computer Engineering
University of British Columbia
Vancouver, Canada
jurij@ece.ubc.ca

***Abstract*—Converter-interfaced resources (CIRs) are multi-timescale systems with dynamics ranging from fast (a few microseconds) to slow (several seconds). This paper introduces a direct interfacing technique for an admittance-based aggregated model (DI-ABAM) of grid-following CIRs, enabling simultaneous time- and frequency-domain analyses in nodal-based electromagnetic transient (EMT) simulators. The proposed aggregated model enables efficient analysis of multi-timescale systems, where dynamic interactions between multiple CIRs and the grid can lead to undesirable oscillations. In addition, the direct interfacing of the ABAM eliminates the time-step delays, enabling the use of large simulation time steps and further reducing the computational burden of aggregated models while maintaining accuracy. The computational advantages of the proposed DI-ABAM are demonstrated through EMT simulations in PSCAD.**

***Index Terms*–Admittance-based modeling, aggregated modeling, EMT simulation, grid-following converter, resonance analysis.**

I. INTRODUCTION

The complexity of modern electrical energy systems is increasing with the growing use of renewable and distributed energy resources (R/DERs) as well as emerging loads, such as data centers and electric vehicle charging stations. The integration of such sources/loads has led to a significant rise in the application of power-electronic converter-interfaced resources (CIRs). The dynamic interaction of CIRs with the grid may lead to undesirable oscillations and control-related interactions [1], exhibiting more complex transients that span a wide frequency range. Depending on the system parameters and operating conditions, such interactions may excite both high-frequency (super-synchronous) and low-frequency (sub-synchronous) resonance modes [2], [3], causing significant equipment damage and economic losses. Consequently, the need for simulations in the design and operation of CIR-based systems is becoming increasingly important.

The electromagnetic transient (EMT) simulators, such as state-variable-based programs (e.g., MATLAB/Simulink's Simscape Electrical toolbox and Opal-RT's RT-Lab), as well as nodal-analysis-based programs (e.g., PSCAD/EMTDC and RTDS's RSCAD), can accurately capture both high- and low-frequency transients. However, detailed switching models of multi-CIR systems are computationally expensive and difficult to scale for large networks. Therefore, depending on the study objective, a balance between accuracy and efficiency is often required. To address this, average-value models (AVMs) of voltage-source converters (VSCs) have been developed for system-level studies. By neglecting discrete switching and focusing on slower average dynamics, AVMs enable larger (medium-sized) simulation time steps; thereby, improving computational efficiency. However, the efficient simulation of CIR-dominated power grids remains a challenge, underscoring the need for reduced-order modeling techniques that can be adapted to various scenarios and simulation tools.

Model-order reduction has been introduced for CIR-based systems by aggregating CIRs into an equivalent model that captures their collective dynamics, thereby improving simulation efficiency [4], [5]. The aggregation methods are typically implemented based on AVMs using dependent voltage/current sources at their interfaces with external networks, i.e., indirect interfacing [4]. As a result, a one-time-step delay is often required when implementing such models in specialized simulators. In state-variable-based tools, this delay resolves algebraic loops caused by direct feedthrough components, while in nodal-analysis-based tools with non-iterative solution approach, e.g. PSCAD, it is mandatory to compute the interfacing variables from their values at the previous time step [5], [6]. However, this delay may introduce numerical inaccuracies/instabilities at large time step sizes, undermining the advantages of aggregated modeling.

Furthermore, typical commercial EMT simulators (e.g., PSCAD) are based on discretized nodal equations, where it is not possible to directly extract small-signal information for stability analysis. Thus, the gap between the capabilities of state-variable-based and nodal-analysis-based simulators has motivated the development of the so-called impedance/admittance (immittance)-based models (I/ABMs) for frequency-domain stability analysis. A key advantage of the I/ABM approach is that it enables systematic aggregation of the system components, allowing for efficient simulation and analysis of large-scale CIR-dominated networks [5], [6].

This paper presents the application of a direct interfacing method for an admittance-based aggregated model (DI-ABAM) of grid-following CIRs for resonance analysis in CIR-dominated power grids. The proposed method enables simultaneous efficient time- and frequency-domain analysis within nodal-based EMT simulators. A transfer-function-based aggregated admittance model is developed for a multi-

979-8-3315-8138-1

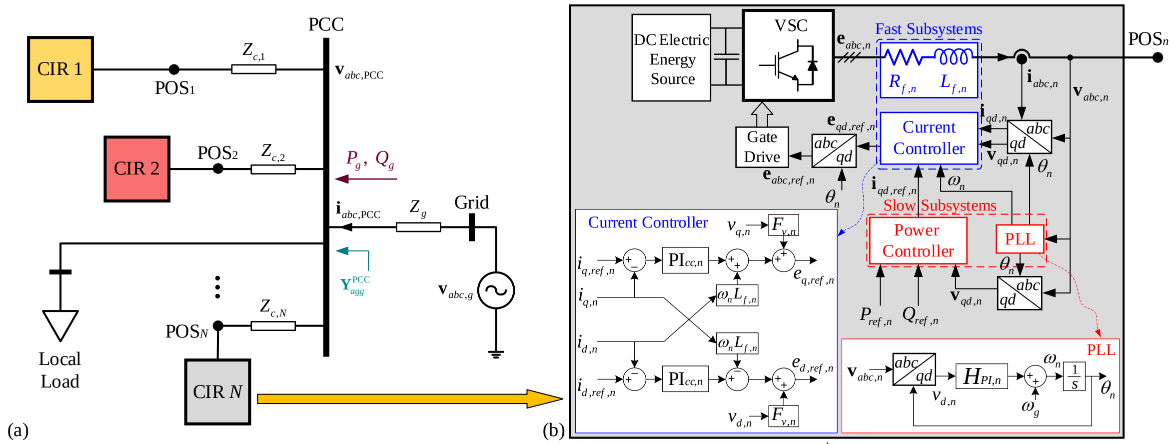

Fig. 1. A multi-CIR system: (a) N grid-following CIRs connected to the PCC, and (b) internal details of the n^{th} grid-following CIR system.

CIR system. The transfer functions of ABAM are discretized and integrated into the overall network nodal equations, enabling a simultaneous EMT solution in PSCAD and eliminating the interfacing delays. It is demonstrated that the proposed DI-ABAM significantly enhances computational performance in simulating multi-CIR systems through aggregation and the use of large simulation time steps, thereby facilitating resonance analysis of evolving power systems.

II. Admittance-Based Aggregated Modeling

A multi-CIR system, as shown in Fig. 1(a), is considered to present the proposed DI-ABAM. This system includes N grid-following CIRs, each interfaced to the point of common coupling (PCC) through a collector line, represented by an impedance $Z_{c,n}$ (i.e., $R_{c,n}$, $L_{c,n}$), where $n\in\{1,\ldots, N\}$. The system may also include local loads connected to the PCC. The PCC interfaces with the grid, represented by its Thevenin equivalent voltages $\mathbf{v}_{abc,g}$ and impedance Z_g (i.e., R_g, L_g).

All the CIRs have an identical structure, as shown in Fig. 1(b) for the n^{th} CIR, although they may have different parameters. Each CIR consists of a synchronous-reference-frame phase-locked loop (SRF-PLL), a qd current controller (with PI controllers), a power controller, and an output RL-filter (i.e., $R_{f,n}$, $L_{f,n}$). The VSC of the CIR is connected through the output filter to the point of synchronization (POS). The SRF-PLL is employed for synchronization, which is fed by the CIR's terminal (POS) voltages $\mathbf{v}_{abc,n}$ [and $\mathbf{v}_{qd,n}$ are the transformed voltages into the CIR's SRF], to estimate the terminal voltage angle θ_n and frequency ω_n.

The CIR output currents $\mathbf{i}_{abc,n}$ are transformed into the CIR's SRF (i.e., $\mathbf{i}_{qd,n}$) using Park's transformation with the PLL output angle θ_n, and are controlled with respect to their reference values, i.e., $\mathbf{i}_{qd,ref,n}$. The reference currents are provided by the power controller based on the active/reactive power set-points ($P_{ref,n}$ and $Q_{ref,n}$) as

$$i_{q,ref,n}=\frac{2}{3}\frac{P_{ref,n}}{v_{q,n}}, \quad i_{d,ref,n}=\frac{2}{3}\frac{Q_{ref,n}}{v_{q,n}}. \tag{1}$$

Without loss of generality, for the purpose of admittance-based aggregation in this paper, it is assumed that the local load in Fig. 1(a) is a constant-impedance load and represented by an equivalent Z_{load} (i.e., R_{load}, L_{load}).

A. Admittance-Based Model (ABM) of Grid-Following CIRs

For the CIR system shown in Fig. 1(b), the current-control loops and the output filter are fast subsystems and can be represented by linear transfer functions/matrices. Also, using the AVM of the VSC and assuming a constant dc-link voltage [3], [4], the nonlinearities due to the switching are removed. Furthermore, the PLL and power controller are slow nonlinear subsystems, and need to be linearized for deriving the ABM [5]. Consequently, the ABM of the entire n^{th} CIR system is obtained in its qd-frame (as detailed in [5]) as

$$\begin{bmatrix}\Delta i_{q,n}\\ \Delta i_{d,n}\end{bmatrix}=\mathbf{Y}_{\text{CIR},n}\begin{bmatrix}\Delta v_{q,n}\\ \Delta v_{d,n}\end{bmatrix}, \tag{2}$$

where the CIR input voltages and output currents are marked with the symbol "Δ" to show the linearization. It is noted that the ABM (i.e., $\mathbf{Y}_{\text{CIR},n}$) of a CIR can be derived analytically when detailed CIR models are available, or numerically when the models are not disclosed by vendors [5].

B. Aggregation of ABMs

The resultant ABM in (2) is in the qd-frame of the corresponding n^{th} CIR, which is synchronized with the estimated angle of its PLL. For simplifying circuit operations and aggregation, the $\mathbf{Y}_{\text{CIR},n}$ in (2) is transformed into a global synchronous frame. Hence, rather than using multiple qd-frames, a common qd-frame synchronized with the grid voltages $\mathbf{v}_{abc,g}$ and the nominal frequency ω_g, is selected as the global qd-frame. The CIR's ABM transformed into the global qd-frame, denoted by $\mathbf{Y}'_{\text{CIR},n}$, is obtained as

$$\mathbf{Y}'_{\text{CIR},n}=\mathbf{T}_{qd,n}\mathbf{Y}_{\text{CIR},n}\mathbf{T}_{qd,n}^{-1}, \tag{3}$$

where

$$\mathbf{T}_{qd,n}=\begin{bmatrix}\cos(\varphi_{0,n}) & \sin(\varphi_{0,n})\\ -\sin(\varphi_{0,n}) & \cos(\varphi_{0,n})\end{bmatrix}, \tag{4}$$

979-8-3315-8138-1

and $\varphi_{0,n}$ is the angle difference between the steady-state value of the estimated angle of the corresponding n^{th} PLL and the global qd-frame angle, obtained from load-flow analysis [3].

Afterward, $\mathbf{Y}'_{\text{CIR},n}$ is inverted and added to its CIR's collector line impedance. The resulting impedance is then inverted once more to obtain the equivalent admittance of the n^{th} CIR and its collector line as

$$\mathbf{Y}_{eq,n}^{\text{CIR}} = \left[\mathbf{Y}'^{-1}_{\text{CIR},n} + \mathbf{Z}_{c,qd,n}\right]^{-1}, \tag{5}$$

where $\mathbf{Z}_{c,qd,n}$ is the n^{th} collector line qd-frame impedance as

$$\mathbf{Z}_{c,qd,n} = \begin{bmatrix} R_{c,n} + sL_{c,n} & \omega_g L_{c,n} \\ -\omega_g L_{c,n} & R_{c,n} + sL_{c,n} \end{bmatrix}. \tag{6}$$

Similarly, the admittance for the equivalent load is derived.

According to the arrangement of the N CIRs, the local load, and their collector lines, as shown in Fig. 1(a), an admittance-based aggregated model (ABAM) seen from the PCC is obtained in form of a transfer matrix as

$$\mathbf{Y}_{agg}^{\text{PCC}} = \sum_{n=1}^{N}\left(-\mathbf{Y}_{eq,n}^{\text{CIR}}\right) + \mathbf{Y}_{\text{Load}}. \tag{7}$$

It is noted that the convention used in Section II–A for the ABM of CIR is based on the generating mode; therefore, the CIRs' ABMs are incorporated into (7) with a negative sign to align with the consuming convention, similar to the load.

C. Proposed Directly Interfaced ABAM

The derived ABAM of the multi-CIR system for direct interfacing in nodal-based EMT simulators (such as PSCAD) must be integrated into the network nodal equation, which is formulated as $\mathbf{G}\,\mathbf{v}(t) = \mathbf{i}(t) + \mathbf{h}(t)$ [7], or equivalently

$$\mathbf{i}(t) = \mathbf{G}\,\mathbf{v}(t) - \mathbf{h}(t). \tag{8}$$

In (8), $\mathbf{G}$ is the network conductance matrix, $\mathbf{v}(t)$ represents the vector of node voltages in the network, and $\mathbf{i}(t)$ and $\mathbf{h}(t)$ are the vectors of the injected current sources and history terms at the network's nodes, respectively.

The transfer-function-based ABAM (in s-domain) derived in Section II–B is discretized and transformed into z-domain using an appropriate integration rule with time-step size Δt, by replacing the variable "s" with $f(\Delta t, z)$, where f depends on the selected integration rule. This results in the admittance-based relationship in the z-domain between the qd-axes voltages and currents of the aggregated model at the PCC as

$$\begin{bmatrix} \Delta i_{q,\text{PCC}}^{g} \\ \Delta i_{d,\text{PCC}}^{g} \end{bmatrix} = \mathbf{Y}_{agg}^{\text{PCC}}(z) \begin{bmatrix} \Delta v_{q,\text{PCC}}^{g} \\ \Delta v_{d,\text{PCC}}^{g} \end{bmatrix}, \tag{9}$$

where

$$\mathbf{Y}_{agg}^{\text{PCC}}(z) = \begin{bmatrix} \dfrac{B_{qq}}{A_q} & \dfrac{B_{qd}}{A_q} \\ \dfrac{B_{dq}}{A_d} & \dfrac{B_{dd}}{A_d} \end{bmatrix}, \quad \frac{B_{xy}}{A_x} = \frac{\sum_{k=0}^{N_{z,xy}} b_{xy,k}\, z^{-k}}{\sum_{k=0}^{N_{p,x}} a_{x,k}\, z^{-k}}. \tag{10}$$

In (9), the superscript "g" indicates that the variables are in the global qd-frame. It is noted that each entry of the aggregated matrix $\mathbf{Y}_{agg}^{\text{PCC}}(z)$ may have a unique transfer function; thus, a common denominator is derived (A_q and A_d) and used for each qd-axes equation to simplify the direct interfacing process. In (10), x and y can be each of the qd-axes. Also, $N_{z,xy}$ and $N_{p,x}$ denote the order of the transfer function's numerator/ denominator, respectively.

To extract the equivalent conductance matrix and history terms for the discretized ABAM, the inverse z-transform is applied to (9), (10), where z^{-1} becomes a delay with interval Δt in the time domain. After cross-multiplication, (9) and (10) are expressed in the time domain (for q-axis) as

$$\begin{aligned} &\Delta i_{q,\text{PCC}}^{g}(t) + \sum_{k=1}^{N_{p,q}} \frac{a_{q,k}}{a_{q,0}} \Delta i_{q,\text{PCC}}^{g}(t - k\Delta t) = \\ &\quad \frac{b_{qq,0}}{a_{q,0}} \Delta v_{q,\text{PCC}}^{g}(t) + \sum_{k=1}^{N_{z,qq}} \frac{b_{qq,k}}{a_{q,0}} \Delta v_{q,\text{PCC}}^{g}(t - k\Delta t) \\ &\quad + \frac{b_{qd,0}}{a_{q,0}} \Delta v_{d,\text{PCC}}^{g}(t) + \sum_{k=1}^{N_{z,qd}} \frac{b_{qd,k}}{a_{q,0}} \Delta v_{d,\text{PCC}}^{g}(t - k\Delta t). \end{aligned} \tag{11}$$

The same approach is applied for the d-axis equation [6]. To comply with (8), the qd-axes equations, obtained similarly to (11), are reformulated into the nodal form as

$$\Delta \mathbf{i}_{qd,\text{PCC}}^{g}(t) = \mathbf{G}_{qd}^{\text{ABAM}}\, \Delta \mathbf{v}_{qd,\text{PCC}}^{g}(t) + \mathbf{h}_{qd}^{\text{ABAM}}(t), \tag{12}$$

$$\mathbf{G}_{qd}^{\text{ABAM}} = \begin{bmatrix} \dfrac{b_{qq,0}}{a_{q,0}} & \dfrac{b_{qd,0}}{a_{q,0}} \\ \dfrac{b_{dq,0}}{a_{d,0}} & \dfrac{b_{dd,0}}{a_{d,0}} \end{bmatrix}, \quad \mathbf{h}_{qd}^{\text{ABAM}}(t) = \begin{bmatrix} h_q^{\text{ABAM}}(t) \\ h_d^{\text{ABAM}}(t) \end{bmatrix}, \tag{13}$$

where $h_q^{\text{ABAM}}(t)$ and $h_d^{\text{ABAM}}(t)$ include the history terms, i.e., the solutions at the previous time steps, of the q- and d-axes equations [obtained similarly to (11)], respectively.

The nodal equations in (12), (13) are derived from the variations in the input nodes' voltages. To conform with (8), equation (12) is modified by adding the steady-state values of the qd-axes currents at the PCC (i.e., $\mathbf{I}_{qd0,\text{PCC}}^{g}$ obtained from load-flow analysis) to its both sides, as well as replacing $\Delta \mathbf{v}_{qd,\text{PCC}}^{g}(t)$ with $\left(\mathbf{v}_{qd,\text{PCC}}^{g}(t) - \mathbf{V}_{qd0,\text{PCC}}^{g}\right)$, wherein $\mathbf{V}_{qd0,\text{PCC}}^{g}$ are the steady-state values of the qd-axes PCC voltages, as

$$\mathbf{i}_{qd,\text{PCC}}^{g}(t) = \mathbf{G}_{qd}^{\text{ABAM}}\, \mathbf{v}_{qd,\text{PCC}}^{g}(t) + \mathbf{H}_{qd}^{\text{ABAM}}(t), \tag{14}$$

where

$$\mathbf{H}_{qd}^{\text{ABAM}}(t) = \mathbf{h}_{qd}^{\text{ABAM}}(t) - \mathbf{G}_{qd}^{\text{ABAM}} \mathbf{V}_{qd0,\text{PCC}}^{g} + \mathbf{I}_{qd0,\text{PCC}}^{g}. \tag{15}$$

The nodal equations in (14), (15) are obtained in the global qd-frame. However, the ABAM needs to be interfaced with the external network in the abc coordinates; thus, (13)–(15) are transformed into abc-frame using Park's transformation, i.e., $\mathbf{K}\left(\theta_g\right)$ where $\theta_g = \int \omega_g\, dt$. Thus, the interfacing equation for the ABAM is constructed in the abc-frame as

$$\mathbf{i}_{abc,\text{PCC}}(t) = \mathbf{G}_{abc}^{\text{ABAM}}(t)\, \mathbf{v}_{abc,\text{PCC}}(t) + \mathbf{H}_{abc}^{\text{ABAM}}(t), \tag{16}$$

where

$$\mathbf{G}_{abc}^{\text{ABAM}}(t) = \mathbf{K}^{-1}\left(\theta_g\right) \mathbf{G}_{qd}^{\text{ABAM}} \mathbf{K}\left(\theta_g\right), \tag{17}$$

$$\mathbf{H}_{abc}^{\text{ABAM}}(t) = \mathbf{K}^{-1}\left(\theta_g\right) \mathbf{H}_{qd}^{\text{ABAM}}(t). \tag{18}$$

The conductance matrix $\mathbf{G}_{abc}^{\text{ABAM}}$ in (17) and the vector of history terms $\mathbf{H}_{abc}^{\text{ABAM}}$ in (18) are incorporated into the overall network nodal equation. Therefore, with the proposed direct interfacing approach, the entire CIR-based system shown in Fig. 1(a) is represented by a single ABAM interfaced through only three electrical nodes at the PCC, that provides a simultaneous solution with the rest of the external network.

D. Proposed Numerical Frequency-Domain Analysis

In addition to the time-domain analysis described in Section II–C, the proposed ABAM is employed for frequency-domain analysis of CIR-based systems. To perform such studies, the total system admittance matrix seen from the PCC is obtained in the global *qd*-frame as

$$\mathbf{Y}_{tot} = \mathbf{Y}_{agg}^{\mathrm{PCC}} + \mathbf{Y}_{g,qd}\,, \qquad \mathbf{Y}_{g,qd} = \left[\mathbf{Z}_{g,qd}\right]^{-1}, \tag{19}$$

where the grid impedance $\mathbf{Z}_{g,qd}$ is obtained similar to (6).

Therefore, according to the admittance-based stability criterion [8], the system's eigenvalues are the roots of $\det\left(\mathbf{Y}_{tot}\right)$. If all roots are located in the left-half plane, the system is stable; otherwise, it is unstable. This approach also enables the analysis of emerging sub- and super-synchronous oscillations through investigating the system's eigenvalues, and can be regarded as an add-on feature of the proposed DI-ABAM method for nodal-analysis-based EMT simulators.

The aggregation of ABMs in Section II–B, the summation of the admittance matrices, and the calculation of the determinant of (19) result in high-order transfer functions. For example, with the original transfer functions of the CIR's ABM in (2), i.e., $\mathbf{Y}_{\mathrm{CIR},n}$ which is a transfer matrix, when the numerator order is n_z=3 and denominator order is n_p=4, even when aggregating just one CIR and one collector line, the resulting order can exceed 90 (after inverting the ABM and combining it with the collector line's IBM). Therefore, model-order reduction is applied to facilitate the implementation of ABAMs in simulation programs, where operations involving high-order transfer functions may become challenging.

For this purpose, the frequency-domain characteristics of the I/ABMs of CIRs, collector lines, loads, and any other system components that can be represented by I/ABMs are determined. Specifically, in MATLAB, the functions "`bode`" and "`frd`" are used to convert Laplace-domain I/ABMs into the frequency domain and generate their frequency-response data, respectively. Subsequently, the I/ABM calculations are carried out numerically at each stage based on their frequency-response data across the desired frequency range.

After deriving the ABAMs' frequency characteristics, the function "`tfest`" is utilized to estimate/fit the frequency response of the resultant ABAM using transfer functions, where the order of their numerator (n_z) and denominator (n_p) can be selected. The suitable order that preserves the characteristic of the ABAM is determined by reducing the orders and choosing the minimum order which remains close to the original characteristic with acceptable accuracy.

III. Computer Studies

Here, the performance of the proposed DI-ABAM is assessed through both time-domain and frequency-domain analyses. The system in Fig. 1(a) with two (N=2) grid-following CIRs is implemented in PSCAD. For comparison, both the non-aggregated AVMs and the proposed DI-ABAM are implemented using the PSCAD/EMTDC library and its custom model-building features, respectively. The system parameters are listed in the Appendix (Tables II and III). It is assumed that the CIRs have different parameters, with CIR-1 using parameter set–A and CIR-2 using parameter set–B.

For the AVMs, the CIRs are interfaced with the external network at their POSs through controlled voltage sources placed behind the output filters. In PSCAD, a one-step interfacing delay is required for interfacing controlled sources, which affects the solution of the non-aggregated AVMs. In contrast, the derived conductance matrix and history terms in the DI-ABAM are integrated directly into the network nodal equation without any interfacing delays, as described in Section II–C. It is also noted that Gear's second-order integration rule is used for discretization [6]. Thus, the transfer functions' orders in (9), (10) become 16 in the *z*-domain.

A. Time-Domain and Frequency-Domain Analyses

The system of Fig. 1(a) is assumed to initially operate in a steady state, defined by the active and reactive power generated/consumed by the CIRs at their POSs: i.e., $P_{ref,1}$ = 21.5 kW, $Q_{ref,1}$ = 4.5 kVAR (generating), $P_{ref,2}$ = -26 kW, and $Q_{ref,2}$ = -2.9 kVAR (consuming), as well as the active and reactive power consumed by the local load, i.e., P_{load} = 2 kW and $Q_{\mathrm{load},}$ = 0.5 kVAR. At t=0.05 s, a small perturbation is applied, and the amplitude of the grid voltages increases by 1%. The transient response of variables at the PCC is shown in Fig. 2, where a very small time step of Δt=1 μs is used in the simulations to ensure numerically accurate results. As observed in Figs. 2(a)–(d), the proposed DI-ABAM effectively captures the resonant dynamics of the original system, consistent with those of the non-aggregated AVMs.

Fig. 3 shows the roots of $\det\left(\mathbf{Y}_{tot}\right)$. Although all the roots are on the left-half plane, and the system is stable, a pair of them is very close to the imaginary axis. As depicted in Fig. 3, the frequency of those roots close to the imaginary axis is ~(889.18/2π) 141.5Hz, close to the oscillation frequency (1/0.0071=140.8Hz) shown in Fig. 2 that is decaying.

B. Computational Performance

The proposed DI-ABAM is benchmarked against the non-aggregated AVM for computational performance. The models are implemented in PSCAD version 5.0 on a computer with a 12th Gen Intel(R) Core(TM) i7-12700 2.1 GHz processor. The study from Section III–A with N=2 is considered, and the simulation is run for 20 seconds. Table I presents the CPU time required by the models for different time step sizes. It is noted that the largest reasonable time-step size for EMT simulations is determined based on the highest frequency required to be captured as $\Delta t_{max} < 1/(10\, f_{max})$ [5], e.g., Δt_{max} = 500 μs for f_{max} = 200 Hz.

As seen in Table I, the DI-ABAM outperforms the non-aggregated AVM by reducing CPU time, i.e., 20.13 s vs. 38.41 s with Δt=5 μs, and 1.31 s vs. 2.01 s with Δt=100 μs. Also, for time steps larger than ~100 μs, the non-aggregated AVM fails to produce numerically reliable results, due to their interfacing delay. However, the DI-ABAM provides valid results with a reduced CPU time of 0.31 s at Δt=500 μs, verifying its efficiency while maintaining acceptable accuracy through removing the interfacing delay.

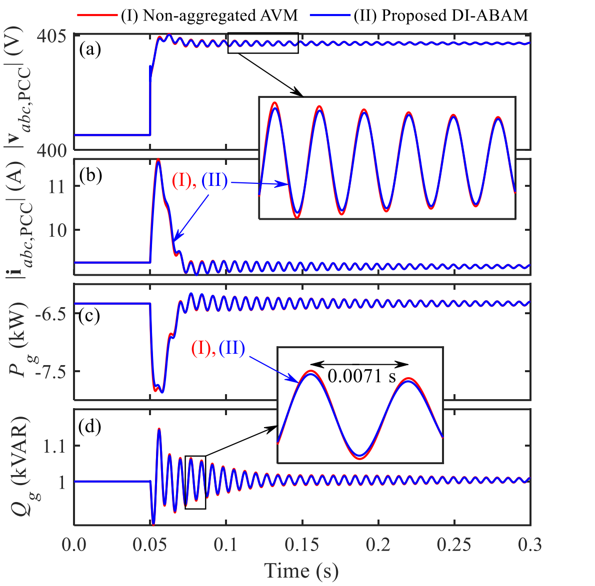

Fig. 2. Transient response of variables at PCC obtained by the subject models, following a voltage perturbation with 0.01 pu magnitude at t=0.05s: (a) magnitude of PCC line voltages, (b) magnitude of PCC currents, (c) active and (d) reactive power delivered by the grid.

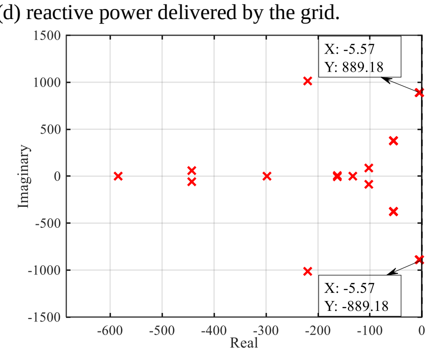

Fig. 3. Roots of $\det\left(\mathbf{Y}_{tot}\right)$ obtained using the admittance-based approach.

To assess the impact of increasing the number of system components on the computational performance of the subject models, the number of CIRs and loads is increased to 20 (i.e., N=20, with 10 CIRs using parameters from set–A and 10 CIRs using parameters from set–B). The CPU times for N=20 CIRs are also listed in Table I.

As shown in Table I, the DI-ABAM shows a significant improvement in computational efficiency over the non-aggregated AVM when N=20 (e.g., 21.48 s vs. 189.29 s with Δt=5 μs, and 1.32 s vs. 9.73 s with Δt=100 μs). Moreover, the processing time for the DI-ABAM with N=20 CIRs remains comparable to that with N=2 CIRs (e.g., 21.48 s vs. 20.13 s with Δt=5 μs, and 1.32 s vs. 1.31 s with Δt=500 μs). This consistent CPU time is a result of applying the same modeling approach and order-reduction procedure in both cases, resulting in only one aggregated admittance model.

IV. Conclusion

In this paper, a direct interfacing approach for admittance-based aggregated modeling (DI-ABAM) of multiple grid-following converter-interfaced resources (CIRs) was proposed to improve the efficiency of time-domain analysis for emerging sub- and super-synchronous oscillation issues in multi-CIR systems. The approach involves deriving admittance-based models for individual CIRs and then numerically aggregating them with the impedance/admittance models of other system components in the frequency domain. The resulting transfer functions of the aggregated model were discretized and incorporated into the overall network nodal equations to enable a simultaneous EMT solution. It was demonstrated that the resulting ABAM can be directly utilized in admittance-based stability analysis, thereby setting the stage for enabling eigenvalue/small-signal analysis of evolving CIR-based grids within nodal-analysis-based EMT simulators. It was verified that the DI-ABAM significantly improves the computational efficiency over non-aggregated average-value models by reducing the CPU time through model aggregation and enabling larger time steps, supporting resonance analysis in CIR-dominated power systems.

TABLE I. Computational Performance of the Subject Models in PSCAD Simulations for N=2 and N=20 CIRs

Model	**Non-aggregated AVM**		**Proposed DI-ABAM**	
Time step	**CPU Time N=2**	**CPU Time N=20**	**CPU Time N=2**	**CPU Time N=20**
5 μs	38.41 s	189.29 s	20.13 s	21.48 s
50 μs	4.08 s	20.22 s	2.54 s	2.67 s
100 μs	2.01 s	9.73 s	1.31 s	1.32 s
500 μs	Not Valid	Not Valid	0.31 s	0.33 s

Appendix

TABLE II. Power Grid Data

Parameter	**Value**	**Parameter**	**Value**
$\lvert \mathbf{v}_{abc,g} \rvert^{\text{Line}}$	400 V	ω_g	2π60 rad/s
R_g, L_g	10 mΩ, 0.8 mH	R_{load}, L_{load}	30 Ω, 4 mH
$R_{c,1}$, $L_{c,1}$	30 mΩ, 0.1 mH	$R_{c,2}$, $L_{c,2}$	20 mΩ, 0.06 mH

TABLE III. Parameter Sets for CIRs

Parameter	**Set–A**	**Set–B**
S_{rated}	16 kVA	12 kVA
V_{rated}, V_{dc}	400 V, 800 V	400 V, 800 V
R_f, L_f	1 mΩ, 1 mH	5 mΩ, 3 mH
K_{pi}, K_{ii}	0.4, 60	0.9, 120
F_v	0.6	0.5
$K_{p,\text{PLL}}$, $K_{i,\text{ PLL}}$	0.8, 3000	4.4, 2800

References

[1] S. H. Maleki, A. Rabiei, B. Yancey, and A. Shojaei, “Stability analysis of grid-forming inverters and converter-based dominated loads for grid of future with beyond inertia feature,” in *Proc. IEEE Power & Energy Society General Meeting (PESGM)*, 2024, pp. 1–5.

[2] Z. Miao, “Impedance-model-based SSR analysis for type 3 wind generator and series-compensated network,” *IEEE Trans. Energy Conv.*, vol. 27, no. 4, pp. 984–991, Dec. 2012.

[3] C. Zhang, M. Molinas, A. Rygg, and X. Cai, “Impedance-based analysis of interconnected power electronics systems: Impedance network modeling and comparative studies of stability criteria,” *IEEE J. Emerg. Sel. Topics in Power Electro.*, vol. 8, no. 3, pp. 2520–2533, Sep. 2020.

[4] A. Safavizadeh *et al.*, “Admittance-based aggregated modeling of converter-interfaced resources with heterogeneous parameters for transient analysis of multi-converter systems,” *IEEE J. Emerg. Sel. Topics in Ind. Electron.*, vol. 6, no. 1, pp. 295–307, Jan. 2025.

[5] A. Safavizadeh, A. Kaushik, S. Ebrahimi, and J. Jatskevich, “Aggregated and reduced-order admittance-based modeling for efficient small-signal analysis of power-electronic-based power systems,” *IEEE Open J. Power Electron.*, vol. 6, pp. 1438–1452, Aug. 2025.

[6] A. Safavizadeh, R. R. Ramesh, S. Ebrahimi, and J. Jatskevich, “Direct interfacing of admittance-based aggregated models of converter-interfaced resources in nodal analysis EMT simulators,” in *Proc. 7th Global Power, Energy Commun. Conf. (GPECOM)*, 2025, pp. 565–571.

[7] H. W. Dommel, *Electromagnetic Transients Program (EMTP): Theory Book*. Bonneville Power Administration, 1995.

[8] L. Fan and Z. Miao, “Admittance-based stability analysis: Bode plots, Nyquist diagrams or eigenvalue analysis,” *IEEE Trans. Power Syst.*, vol. 35, no. 4, pp. 3312–3315, Jul. 2020.